Characterizing Internally Mixed Insoluble Organic Inclusions in Aqueous Aerosol Droplets and Their Influence on Light Absorption

Adèle M. C. Laurain and Jonathan P. Reid*

School of Chemistry, University of Bristol, Bristol BS8 1TS, U.K.

Received: March 13, 2009; Revised Manuscript Received: May 5, 2009

A strategy is developed for characterizing the properties and microphysical structure of a mixed phase aerosol droplet consisting of an aqueous sodium chloride host and an insoluble organic inclusion using aerosol optical tweezers and Raman spectroscopy. In particular, palmitic acid (PA), solvated in ethanol and nebulized to produce a flow of aerosol, is coalesced with an optically trapped sodium chloride droplet. Once the ethanol solvent has evaporated, a hydrated crystalline organic phase is formed. Two distinct classes of mixed phase structure are observed. The observation of a PA aggregate formed immediately on coalescence at the surface of the host droplet is consistent with the hydrophobicity of the organic component; this is the dominant structure observed. However, PA inclusions are also observed within the droplet bulk following the evaporation of the ethanol solvent. This may be attributable to the interplay of the optical forces exerted on the inclusion and the lowering of the surface tension of the aqueous droplet by the presence of a monolayer of PA, or through direct incorporation of a PA inclusion by impaction. In this latter class of structure, an autocorrelation analysis of the Raman signatures suggests that the inclusion diffuses throughout the entire droplet volume. Finally, the coupling of nonresonant and resonant heating of the droplet, arising from motion of the PA inclusion within the droplet, is contrasted with observations of the lowering of equilibrium droplet size that accompanies the presence of a weakly absorbing inclusion, a polystyrene bead, within the droplet core.

1. Introduction

There is considerable interest in the optical, physical, and chemical properties of atmospheric aerosols.[1,2] Particles are complex in composition, containing both inorganic salts and organic components.[3] Field measurements have enabled the characterization of water-soluble and -insoluble organics in marine aerosol and have revealed the presence of surface active components that are expected to form films at the surfaces of aerosol particles,[4] affecting the thermodynamic properties of the aerosol and the kinetics of particle transformation.[5,6] In this study, we use aerosol optical tweezers to characterize aqueous droplets containing water-insoluble organics, specifically the insoluble fatty acid (palmitic acid, PA, $C_{15}H_{31}CO_2H$). PA is found in abundance in samples from marine field measurements[7,8] and has a low solubility in water at 20 °C (~30 μM).[9] We focus particularly on the formation and dynamics of an insoluble PA inclusion and contrast the behavior of such a nonspherical nonabsorbing inclusion with a spherical weakly absorbing inclusion, a 500 nm diameter polystyrene bead.

Previous experimental studies of the spectroscopy and dynamics of solid inclusions within liquid droplets have been limited in scope and have largely examined scattering from spherical host droplets containing spherical nonconcentric inclusions. Bronk et al. examined fluctuations in elastic scattering and fluorescence intensity from single aqueous droplets (diameter ~30 μm) doped with ~200 fluorescent spheres (diameter 460 nm).[10] The autocorrelation function of the scattering intensity suggested that motion of the inclusions could be separated into two time scales: a short time scale for diffusion on the length scale defined by the wavelength of the light, and a long time scale attributed to larger displacements of the particles moving within the nonuniform internal light intensity profile within the host.

Videen and co-workers considered the influence of the relative sizes of the inclusion and host on the fluctuations in scattering intensity.[11] For small inclusions relative to the host size, the magnitude of the fluctuations in scattering intensity was found to depend approximately linearly on the geometric cross-section of the inclusion and to increase with the number of inclusions according to a power law dependence, with an exponent that was dependent on the inclusion size. Krieger and Braun used the scattering amplitude to characterize the varying size of a submicrometer solid inclusion during the deliquescence and dissolution of an inorganic solute.[12] Further, fluctuations in scattering intensity were used to discriminate between an inclusion allowed to freely move within the aqueous droplet bulk and an inclusion restricted to motion on the droplet surface.[13] For liquid−liquid phase partitioning, Prabhu et al. modeled light scattering from a droplet of oleic acid (6 μm radius) containing an aqueous inclusion (<2 μm radius).[14] The inclusion was shown to act as a scattering source contributing to the light interference structure, behavior that was found to be consistent with measurements of scattering from oleic acid droplets (~10 μm diameter) containing small micrometer sized water inclusions.[15] Scattering from droplets containing nonspherical inclusions has been treated theoretically,[16] but little experimental work has been undertaken.

Experimental techniques such as acoustic levitation,[17] electrostatic trapping,[18] or optical tweezers[19] allow studies of single aerosol particles. When a droplet passes through a tightly focused laser beam, the optical gradient force draws the particle into the region of highest light intensity, counter to the optical scattering force which acts to dispel the particle from the light beam. If the gradient force dominates the scattering force, the

* To whom correspondence should be addressed.

10.1021/jp902248p CCC: $40.75
Published on Web 05/26/2009

particle is immobilized in a three-dimensional optical trap by a restoring force many orders of magnitude larger than either the scattering or gravitational forces exerted on the particle. Such a trap is referred to as a single-beam gradient force optical trap or *optical tweezers*. The advantages of optical tweezers include the opportunity to simultaneously manipulate multiple particles in the 1−10 μm radius range, to control the coagulation of different aerosol components allowing sequential dosing of trapped particles, and comparative measurements on particles of different composition. Raman spectroscopy can be used to interrogate the particle size, phase, and composition.[20]

In this publication we report on a strategy for the controlled formation of aqueous droplets containing either a nonspherical nonabsorbing insoluble organic inclusion formed from PA or a spherical weakly absorbing polymer bead inclusion. We examine the influence of these two classes of inclusion on the absorption of light by the aerosol and describe the spatially resolved characterization of particle composition by Raman spectroscopy. It is intended that this publication will provide a crucial underpinning for future work to explore the thermodynamic and kinetic factors governing the size of mixed phase particles.

2. Experimental Strategy

The application of optical tweezers to studies of aerosols has been described in detail previously, and only a brief review will be discussed here.[21] The optical trap is formed from a laser operating at 532 nm, which is focused into a custom fabricated cell using an oil immersion objective. Aerosol is generated with a medical nebulizer, and the optical trap captures any droplets drifting within the trapping region. The composition of the initially trapped droplet is equal to the composition of the nebulized solution.[21] The relative humidity (RH) surrounding the trapped particle decreases with time after the nebulization process although it is not measured or controlled in this study. Sodium chloride (purity 99.5%, Fisher Scientific), PA (purity min 99%, Sigma-Aldrich), and absolute ethanol (purity 100%, Hayman Ltd.) are used. In some experiments, polystyrene beads, nominally 500 nm in diameter (Duke Scientific), are also used dispersed in an aqueous solution.

The trapping plane is illuminated by a blue LED, and a brightfield image is collected with a CCD camera. The 532 nm laser acts as the excitation source for performing Raman spectroscopy; the inelastically scattered light from the droplet is collimated by the microscope objective and imaged onto the entrance slit of a spectrograph. The droplets are assumed to be spherical and have sizes within the Mie regime.[22] Thus, the Raman fingerprint consists of a broad underlying spontaneous Raman band that can be used to characterize the composition of a trapped particle and to observe phase changes occurring within the droplet. At wavelengths commensurate with whispering gallery modes (WGMs), the Raman intensity is enhanced and provides a unique fingerprint of droplet size. A WGM occurs at a specific ratio of the droplet radius to wavelength at which the light is able to form a standing wave around the droplet circumference. The size can be determined with nanometer accuracy by comparing the fingerprint of WGMS with Mie scattering calculations.[20,22]

3. Characterizing Mixed Phase Aerosol Particles Using Aerosol Optical Tweezers

In previous work we have demonstrated that the coalescence of aqueous and liquid organic aerosol droplets can be controlled using aerosol optical tweezers.[23,24] The strategy for forming a mixed phase aerosol droplet containing a solid inclusion is based on dosing of a trapped aqueous sodium chloride droplet with either aqueous or organic aerosol containing the dispersed solid inclusion (e.g., polystyrene latex beads) or the solubilized organic (e.g., PA in ethanol). We focus first on the latter system.

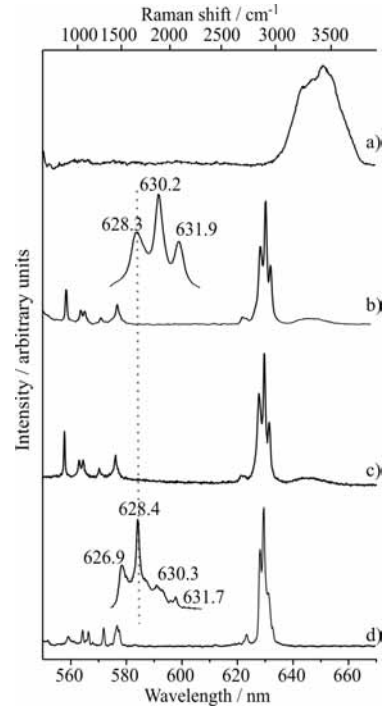

Figure 1. Raman spectra of bulk samples: (a) 20 g/L NaCl solution, (b) absolute ethanol, (c) 0.2 M PA in ethanol, and (d) pure PA powder.

Raman spectra of each of the bulk solutions studied in this work over a range in the Stoke's shift of 800−3700 cm^{-1} are reported in Figure 1, along with a spectrum of PA powder. All spectra were recorded in the backscattering geometry, providing benchmark calibration measurements consistent in polarization with the droplet measurements that will be presented later. The spectra contain both the depolarized and polarization conserved components. The sample is placed on the coverslip and a fluorocarbon oil is used as the immersion oil to provide an unambiguous Raman signature of the sample without the added congestion of features from a hydrocarbon oil. The spectrum in Figure 1a is dominated by the OH stretching band of water between 632 and 660 nm.[25] Spectra 1b and 1d, recorded from absolute ethanol and PA powder, respectively, are dominated by the CH-stretching vibrations. The band structures of the two organics differ markedly, confirming that the alcohol[26] and the fatty acid[27,28] can be distinguished. Spectrum 1c is recorded from a solution of 0.2 M PA in ethanol and resembles that of the pure alcohol. The Raman shifts reported in the literature and in this work are summarized in Table 1 along with spectral assignments.

The low solubility of PA in water prevents direct incorporation within a droplet through nebulization of an aqueous solution. However, PA is considerably more soluble in ethanol, and this has been chosen as an aerosol carrier. The mixed organic/inorganic aqueous droplet is formed in three steps. An aqueous sodium chloride droplet of known concentration (0.34 M) is initially trapped and a Raman spectrum recorded (Figure 2a), allowing the determination of the droplet size from the pattern of WGMs. This allows the initial solute mass loading to be estimated. A solution of PA in ethanol (between 0.1 M and 0.25M) is then nebulized and introduced into the cell

TABLE 1: Experimentally Measured Wavelengths and Raman Shifts (this work) Compared with Reported Raman Shifts (from the literature) and Accompanying Mode Assignments for Palmitic Acid and Ethanol: δ, Bending Mode; ν, Stretching Mode; ρ, Rocking Mode

species	experimental wavelengths/nm	experimental Raman shift/cm^{-1}	Stoke's shift from literature/cm^{-1}	assignment
pure PA powder	559.0	906	909	p(CH_2)[a]
	564.0	1067	1063	v(C−C)[a]
	566.1	1130	1129	
	571.5	1298	1296	δ(CH_2) twist vibrations[a]
	576.2	1441	1421	δ(CH_2) twist vibrations and δ(CH_3) or δ(CH_2) deformations[a]
	576.9	1462	1455	
	626.9	2844	2848−2854	ν(CH_2) sym[b]
	628.4	2883		
	630.3	2931	2915−2924	ν(CH_2) asym[b]
	631.7	2966		
absolute ethanol	558.3	884	882	ν(CC)[c]
	563.7	1056	1051	ν(CO)[c]
	565.5	1093	1096	ρ(CH_3)[c]
	571.0	1282	1282	δOH[c]
	576.7	1457	1453	δ(CH_3) asym[c]
	576.9	1462	1478	δ(CH_3) sym[c]
	628.3	2881	2877	ν(CH_3) sym[c]
	630.2	2928	2928	ν(CH_3) sym, ν(CH_2) asym[c]
	631.9	2970	2972	ν(CH_3) sym[c]
			3342 ± 50	OH stretching vibration[c]

[a] Reference 28. [b] Reference 27. [c] Reference 26.

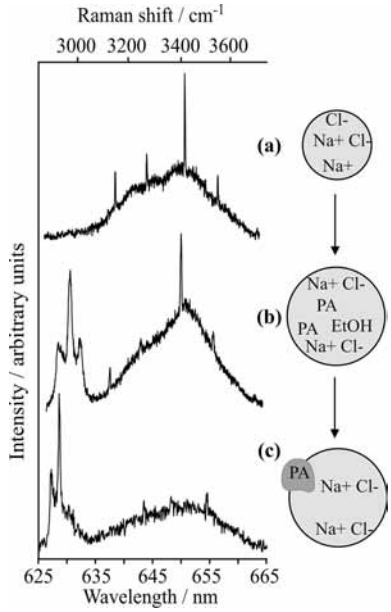

Figure 2. A schematic of the experimental strategy for forming mixed organic/aqueous aerosol when the organic component is insoluble in water. Raman spectra of (a) the initial 20 g/L NaCl droplet, (b) the mixed aqueous/ethanol droplet following dosing of the trapped droplet with palmitic acid/ethanol aerosol, and (c) the mixed phase aqueous sodium chloride/palmitic acid aerosol droplet following the evaporation of the ethanol component.

through an inlet that delivers the aerosol at a distance of ~5 mm from the trapped droplet. Thus, PA solubilized in ethanol is incorporated within the aqueous droplet, leading to the appearance of a CH stretching band in the Raman spectrum similar to the one recorded from bulk ethanol (compare Figures 1b and 2b). The most intense Raman peaks for the two organic components are wavelength resolved (630.2 nm for ethanol and 628.4 nm for PA). Thus, observation and identification of the predominant species is possible.

Immediately following coagulation, the WGMs remain in the spectrum and the size of the doped droplet can be estimated. Thus, the amount of PA/ethanol solution incorporated by coagulation can be estimated from the volume change observed before and after coagulation. A size estimate is possible based on the similarity in the refractive index of the ethanol and aqueous solutions. At 589 nm, the difference in refractive index between a 0.34 M aqueous sodium chloride solution and a 10% v/v ethanol aqueous sodium chloride is 0.001,[9] leading to an error in the size of <0.1% or <5 nm for a 5 μm radius droplet.

Ethanol evaporates on a time scale of tens of seconds from the composite droplet, and this loss rate can be enhanced by forming the composite droplet in a moist nitrogen/water atmosphere. As ethanol evaporates, the contour of the CH stretching band changes, becoming more similar to that observed for pure PA powder (compare Figures 1d and 2c).[27,28] The mass of PA introduced into the host droplet is equivalent to a concentration at the millimolar level, well above the solubility limit of PA in water. The evaporation of the ethanol can be followed from the decrease in intensity of the peak at 630.2 nm with time. As the contribution of the PA component to the CH stretching band becomes increasingly dominant, a PA aggregate forms, and determining the level of ethanol remaining becomes increasingly difficult.

4. Spectroscopic Signatures of the Microphysical Structure of Mixed Phase Particles and Nonresonant Absorption

The particular location of a solid inclusion within a liquid host droplet can lead to distinct spectroscopic signatures. The trapping beam has a focal waist considerably smaller than the droplet diameter and the backscattered Raman light provides a spatially resolved measurement of composition through the central core of the host droplet.[24] An example of the influence of inclusion position on a sequence of Raman signatures is shown in Figure 3 over a period of 6 s. An aqueous sodium chloride droplet was doped with aqueous aerosol containing polystyrene latex beads, 500 nm diameter. The dilution of the aqueous solution of beads was such that only a single polystyrene inclusion was introduced to the trapped droplet after

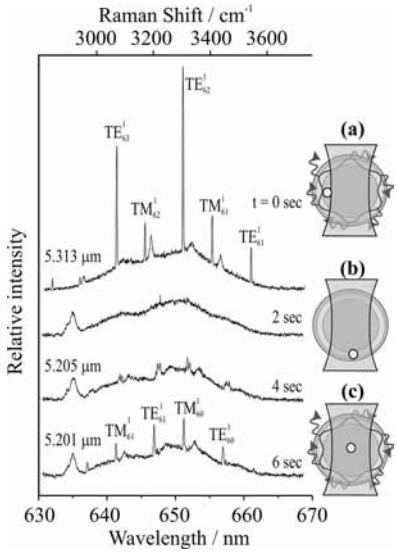

Figure 3. Time dependence in the Raman fingerprint from an aqueous sodium chloride host droplet containing a submicrometer polystyrene bead inclusion. Initially, the inclusion resides out of the WGM volume and the probe laser volume (schematic a), yielding a fingerprint consisting of both stimulated Raman scattering and spontaneous scattering from water and allowing the size of the droplet to be estimated ($t = 0$ s). During the period 2−4 s, the inclusion moves into the laser probe volume and within the WGM volume (schematic b), quenching the WGM structure. At 6 s, the stimulated structure is restored on the OH band, allowing the droplet size to be estimated and providing a spontaneous Raman signature of the polymer bead, consistent with schematic c.

numerous coalescence events, and the inclusion was clearly visible in the video microscopy.

At $t = 0$ s, the position of the inclusion is consistent with schematic a, with the WGM volume undisturbed by the inclusion, which is residing off-axis from the laser beam. However, when the inclusion is located within the WGM volume, the quality factor of the WGM is reduced and the amplification of the Raman signature is quenched, as indicated in schematic b.[29−31] Under these circumstances, the size of the droplet host cannot be determined. If the inclusion resides at the top or bottom of the droplet, on the axis of the laser beam, a spontaneous Raman band from the inclusion is observed, as recorded by the appearance of a signature of C−H stretching vibrations in the spectra at 2 and 4 s. If the inclusion resides toward the center of the droplet, then the amplification of the Raman signature at WGM wavelengths is restored and a spontaneous signature is also observed, schematic c, as observed at 6 s.

The complex part of the refractive index of polystyrene is $\sim 5 \times 10^{-4}$ at 532 nm,[32] considerably higher than the value of the salt solution (containing low concentrations of impurities) that we have determined ($\sim 5 \times 10^{-9}$).[33] Assuming that the absorption can be treated by the Beer−Lambert law, a reasonable assumption given that the whole beam intensity passes through the droplet, the temperature elevation of an undoped droplet can be estimated from the equation[33]

$$\Delta T = \frac{(1 - \exp(-2R_d\alpha)) \times P}{4\pi R_d K_a} \quad (1)$$

where α is the absorption coefficient, R_d is the droplet radius, P is the laser power illuminating the droplet, and K_a is the thermal conductivity of air (25.8×10^{-3} W m^{-1} K^{-1} at 295 K and 100 kPa). This is an appropriate treatment for the case of nonresonant heating, for which the path length of the light through the particle is governed by the droplet diameter.

When the inclusion resides outside the trapping beam path, the droplet temperature can be estimated to be ∼6 mK above the ambient temperature for a typical trapping power of 10 mW and assuming that the absorption coefficient is $\sim 1 \times 10^{-3}$ cm^{-1}.[33] From a volume-weighted effective medium treatment of the refractive index of the droplet, the absorption coefficient can be estimated to rise to $\sim 1.3 \times 10^{-2}$ cm^{-1} when the inclusion resides within the beam profile, giving rise to a temperature increase of ∼80 mK. By applying the treatment described in our earlier publication,[33] we can estimate that the decrease in equilibrium size determined from the spectroscopy when the inclusion moves into the laser beam path (from 5.31 to 5.20 μm) is consistent with a temperature change of ∼60 mK, similar in magnitude to the estimated level of heating. Given the approximations inherent to this treatment, agreement within the same order of magnitude is acceptable.

A PA inclusion within a host aqueous sodium chloride droplet, unlike the polystyrene inclusion, can be assumed to approximate to a nonabsorbing inclusion at the wavelength of 532 nm, and the level of nonresonant absorption is determined purely by the aqueous component and impurities.[33] Thus, we would expect the volume of water associated with the particle to be determined by the solution thermodynamics and the surrounding RH, and to not be susceptible to significant temperature fluctuations as PA diffuses within the host droplet.

In Figure 4, we compare the spectroscopic signatures and brightfield images recorded prior to and following a coagulation event, including a bulk Raman spectrum of ethanol for comparison with the CH stretching band contour recorded from the droplet. The droplet radius prior to dosing with the ethanol/PA aerosol was 4.53 μm. In this experiment, an aggregate was observed almost immediately following coagulation. Although the brightfield image is a two-dimensional projection of a three-dimensional structure,[23] the aggregate extends into the gas phase, beyond the boundary of the aqueous phase, appearing to reside on the edge of the droplet throughout the measurement. Indeed, the aggregate circulates on a locus defined by the droplet circumference, confirming that the aggregate resides at the surface. The rate of rotation is very slow ($\ll$1 Hz), sporadic and variable in direction, suggesting that the aqueous host droplet and PA inclusion remain in a stable configuration and that there is no persistent rotation of the host droplet within the trapping beam. At all times, the Raman signature of the mixed phase particle does not show resonant enhancement at WGM wavelengths, although a clear Raman signature from PA is observed, even at the earliest times. Thus, not only is ethanol rapidly lost from the droplet and the aggregate formed almost instantaneously on coalescence, but the aggregate resides on the surface quenching the resonant structure (cf. Figure 3b). Further, the geometric extent of the inclusion is sufficiently large that it extends onto the axis of the droplet probed by the laser yielding the distinct Raman signature of PA.

The aggregate can also be formed in the core of the droplet and subsequently remains in the bulk, as illustrated in Figure 5. In this second case, the circumference of the droplet is unaffected by the inclusion, and the resonant structure at WGM wavelengths is apparent in the Raman fingerprint. The pattern of WGMs remains consistent with an homogeneous droplet, rather than a core−shell structure, and the droplet size can be determined accurately. The characteristic signature of ethanol,

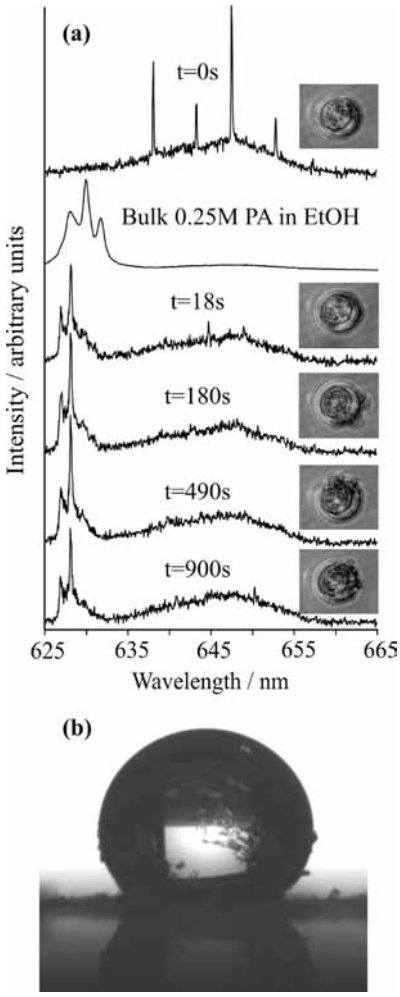

Figure 4. (a) Raman spectra and images of a 0.34 M aqueous NaCl droplet before and following dosing with a solution of 0.25 M PA in ethanol. The formation of PA inclusion on the edge of the droplet shortly after dosing is apparent from the images. The Raman fingerprint of the nebulized ethanol/PA solution is shown for comparison, suggesting that the CH signature arises from the PA component alone. (b) Image of an aqueous sodium chloride droplet resting on a palmitic acid surface for droplet shape analysis.

while intense immediately after the collision, diminishes and the peak characteristic of PA remains visible until the conclusion of the experiment. Even though the inclusion remains located in the droplet center, the spontaneous Raman intensity from the PA is much lower than that observed in the first example (Figure 4), suggesting that the PA inclusion is lower in volume fraction within the probe volume.

The observations of inclusion location reported in Figures 3, 4, and 5 can be summarized as follows. The commercial polystyrene latex beads used in this work are spherical and dispersed in an aqueous medium stabilized by the presence of a surfactant. Contact angle measurements reveal that water only partially wets a polystyrene surface with a contact angle of ~85°,[34] but the presence of the surfactant is anticipated to enhance wetting. Thus, a polystyrene inclusion in an aqueous droplet is expected to be free to move within the entire droplet volume, consistent with our observations. The influence of optical forces on the inclusion cannot be ignored when considering the observation of the long-time stability of the polystyrene bead within the droplet core following the measurements reported in Figure 3.

The PA inclusion is observed to reside at the surface of the droplet in Figure 4 but within the host for the experiment

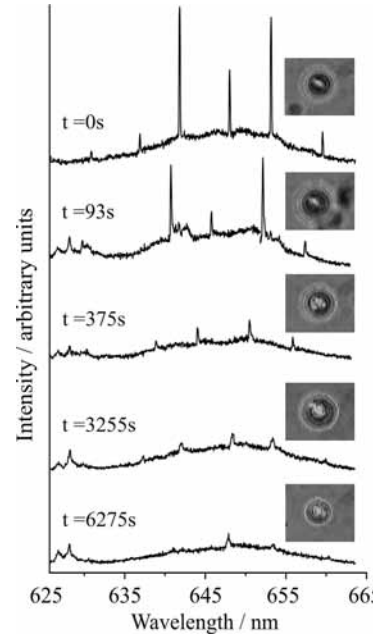

Figure 5. Raman spectra and images of a 0.34 M aqueous NaCl droplet before and following dosing with a solution of 0.25 M PA in ethanol. The formation of PA inclusion within the center of the droplet shortly after dosing is apparent as an increase in the level of green light scattering along the central axis of the droplet through which the laser beam passes. The location of the inclusion within the host does not inhibit the appearance of the stimulated Raman scattering signal, although it is diminished in intensity.

presented in Figure 5. Repeated experiments suggest that the former is dominant but that the latter is occasionally observed. The concentration of PA in the host droplet is at the millimolar level, many orders of magnitude higher than the solubility limit at 20 °C. The Kraft temperature of PA in water[35] is 45 °C, and thus the aggregate formed is expected to be a hydrated crystalline phase at the temperature of this study. Further, contact angle measurements of aqueous sodium chloride (0.34 M) on a PA powder confirm the hydrophobicity of the surface with a contact angle >100°, consistent with previous wettability studies of the work of adhesion of water on a PA surface,[36] which yielded a contact angle of 108°. Thus, the apparent stability of the PA inclusion on the droplet surface is consistent with this observation. In Figure 4b we show an image from a contact angle measurement using a droplet shape analysis system (Krüss DSA100), which shows not only the hydrohobicity of the PA surface but illustrates the migration of a PA crystal onto the surface of the droplet.

The presence of a small PA inclusion within the host droplet in Figure 5 suggests that the inclusion may form within the droplet or be directly incorporated by impaction. This is to be contrasted with the immediate identification of a large crystalline PA inclusion at the surface of the droplet in the measurement reported in Figure 4. Reduction of the surface tension of water to 56 mN m^{-1} when covered with a complete monolayer of PA[37] may lower the thermodynamic driving force for the inclusion to reside at the surface, although resolving this factor from the influence of optical forces on the inclusion is not possible at this stage. We consider the motion of the PA inclusion within the host more fully in the next section.

5. Measurements of Internal Diffusional Dynamics and Resonant Absorption

Fluctuations over short time in the intensity of Raman scattering from the different components can be used to

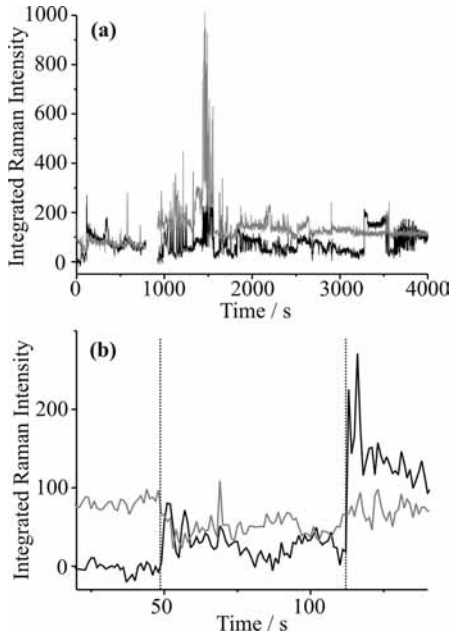

Figure 6. (a) Integrated Raman intensity of the CH stretching signature of PA (black line), centered on 628.4 nm, and of the OH stretching signature of water (gray line), centered on 646.9 nm. (b) An expanded view of the integrated Raman intensities at the time of the coagulation event, indicated by the dashed line.

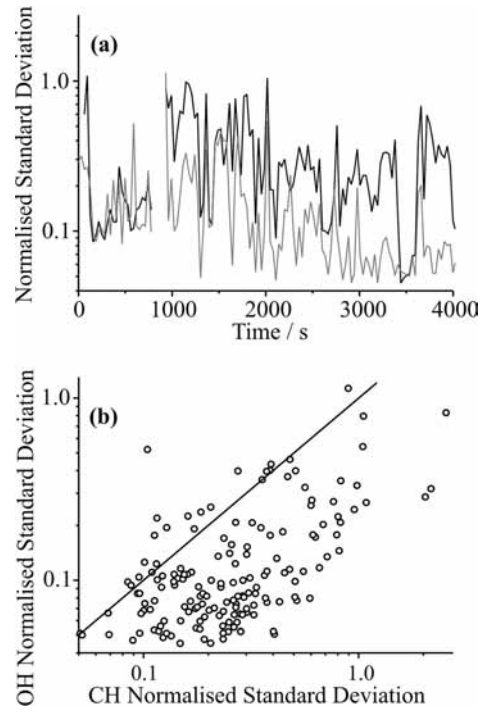

Figure 7. (a) The time dependence of the standard deviation of the Raman intensity over 30 s intervals, compared to the mean intensity within each time window. Fluctuations in the signal from the PA component are indicated by the black line and from water by the gray line. (b) Correlation between the standard deviations in the Raman signal from the PA and water components.

interrogate inhomogeneities in the composition along the trapping beam axis. The time dependence of the Raman signatures is reported in Figure 6a, presenting background corrected integrated intensities around the characteristic wavelengths of 628.4 nm (PA/ethanol) and 646.9 nm (water). An expanded view, just prior to and post coagulation, is shown in Figure 6b. In this experiment, the PA inclusion resides within the droplet core, resonant structure is retained throughout the run, and the size of the host can be monitored. The host droplet size is estimated to decrease from 4.55 to 4.33 μm over the first 700 s following coagulation. Between 700 and 900 s the droplet is dosed with further aqueous sodium chloride droplets, increasing the droplet size to 5.75 μm at ~900 s. The droplet size then steadily declines to ~4.35 μm over the following 4000 s.

The initial coalescence of the aqueous and ethanol droplets occurs between times of 49 and 50 s. Prior to coagulation, the intensity of the Raman CH signal is zero and fluctuations of the OH (and CH) integrated intensity arise from fluctuations in laser power and detector noise. After coagulation, the CH signal intensity rises instantaneously, as ethanol and PA are incorporated. A corresponding decrease in OH signal intensity is observed, with the organic components displacing water from the laser beam path along the central vertical axis of the droplet. Large fluctuations persist in the CH signal over ~30 s, and the CH signal decays back toward zero, indicating the rapid evaporation of ethanol. From ~90 to 110 s, the CH and OH signatures are anticorrelated, suggesting that there must be some local fluctuation in the organics-to-water mixing ratio along the trapping beam path. Between 112 and 113 s, the CH intensity suddenly rises and the resonant structure on the spectrum is temporarily quenched. After 113 s, the CH band shape is consistent with the formation of a PA inclusion.

In Figure 7a, fluctuations of the CH and OH signal intensities are compared over sequential 30 s time windows by examining the standard deviation in the signal intensity relative to the mean signal level within each time window (referred to as the normalized standard deviation), an approach similar to that used by Videen et al.[11] Fluctuations in the CH level are strongly correlated to those in the OH signal (Figure 7b). Once the droplet size has increased by further coagulation after ~900 s, fluctuations in the CH signal become considerably more pronounced relative to those from OH, apparent from the correlation appearing below the 1:1 line. The larger water volume leads to a more stable OH signature. Conversely, the PA inclusion is able to move further off the laser beam axis, leading to greater fluctuations in the CH signal level. This is qualitatively consistent with previous work, which has shown that the amplitude of fluctuations decreases as the inclusion size becomes comparable to the host.[11]

The Brownian diffusion of the inclusion within the host leads to temporal variability in the position of the inclusion and, thus, fluctuations in the intensity of backscattered Raman light. Further, rotational diffusion of the whole particle within the trap can lead to fluctuations in scattering intensity.[18] Previous measurements have shown that the rotational Brownian motion of a solid particle leads to correlations in intensity fluctuations on time scales shorter than 20 ms.[18] Longer time correlations in scattering, on the 1−10 s time scale, were attributed to the nonspherical particle periodically adopting specific orientations, relative to the laser illumination, that showed particular enhancement in the scattering along the optical collection axis, as determined by the particle morphology. The bursts in scattering occurred on a second time scale, determined by rotational Brownian motion, leading to long correlation times.

The autocorrelation function for a data set of intensities, I, and n points over a time period consistent with k points, is defined by eq 2.

$$R(k) = \frac{1}{(n-k)\sigma^2}\sum_{t=1}^{n-k}(I_t - \mu)(I_{t+k} - \mu) \qquad (2)$$

The variance in the signal is represented by σ and the mean by μ. In Figure 8a, the autocorrelation functions calculated from the fluctuations in the CH and OH Raman signals at early times before dosing, after dosing but before inclusion formation, and after inclusion formation are compared. Prior to dosing, fluctuations in the OH intensity are dependent solely on the signal-to-noise of the measurement and the autocorrelation decays rapidly to zero. The CH and OH autocorrelations after dosing show a strongly correlated signal over long times. This is due to the homogeneous mixing of the droplet and the slow evaporation of ethanol accompanied by a decrease in size which occurs on time scales longer than 100 s. As we have no control over the time frame over which the inclusion forms, we are unable to calculate the autocorrelation over a long time window.

Once the inclusion is formed, the CH and OH autocorrelation functions (calculated over the long time series up to 4000 s) continue to show long-time correlated variations in signal. The time scale of correlation is consistent with previous measurements of an inorganic inclusion within a host aqueous droplet, which showed correlation times of 10 to 100 s.[18] Such long correlations can be attributed to the inclusion adopting specific positions within the host droplet, and this is dependent on the slow diffusion of the inclusion within the host particle or rotational diffusion of the whole particle, accompanied by change in the host size. As already stated, the rate of rotational diffusion of the inclusion and host is $\ll 1$ Hz.

Once the inclusion has formed, there is a clear dependence of the autocorrelation on the time window over which it is calculated, as shown in Figure 8b. When the droplet is smallest, between 113 and 613 s, the CH and OH signals show a strong autocorrelation. When the droplet is larger, at all time windows longer than 1113 s, the signals show a weaker autocorrelation. This reflects the change in host size within which the inclusion can move and is consistent with an inclusion that is constrained by the size of the host droplet, with tighter confinement for smaller host size and, thus, smaller fluctuations in signal amplitude.[11]

The typical time scale for free-diffusion of the inclusion, τ, over a length scale characterized by the mean square displacement, $\langle x^2 \rangle$, can be estimated from the relation

$$\tau = \frac{\langle x^2 \rangle 3\pi\eta a}{k_B T} \qquad (3)$$

where η is the viscosity and a is the radius of the inclusion. From the largest to the smallest size of the host, the fractional volume change is a factor of 1.38 which leads to only a marginal change in the concentration and viscosity (<5%) of the solution.[9] On dosing with the ethanol/PA aerosol, the trapped droplet size changes from 4.50 to 4.63 μm. On the basis of this size change, and ignoring changes in partial molar volume of the organic and aqueous components, the mass of PA added can be estimated to be 1.6 pg corresponding to a PA inclusion of radius 0.7 μm if assumed to be spherical, although it should be remembered that a non-spherical hydrated crystal forms. If the characteristic time of the spectroscopic signal correlation is taken as 30 s, the mean displacement during this time would be expected to be 4.1 μm, similar to the difference between the droplet and inclusion radii. Given that the spectral signatures

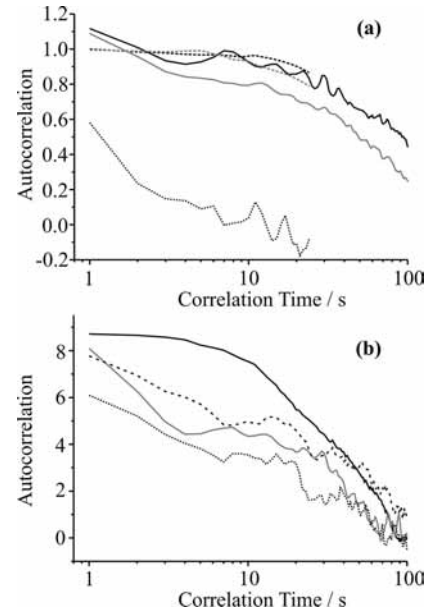

Figure 8. (a) Autocorrelation functions determined from the OH water signature prior to coagulation (dotted gray line), the CH PA (gray dashed line) and OH water (black dashed line) signatures prior to the formation of the inclusion, and the CH PA (gray solid) and OH water (black solid) signatures after the formation of the inclusion. (b) Autocorrelation functions determined from the OH water signature over time windows 113 to 613 s (solid black line), 1113 to 1613 s (solid gray line), 1613-2113 s (dotted gray line), and 2113 to 2613 s (dashed black line).

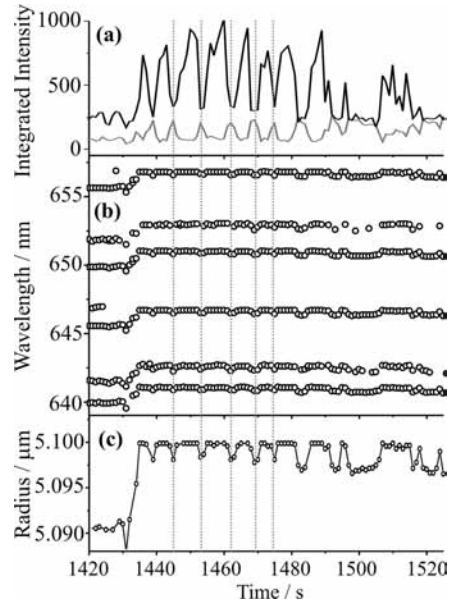

Figure 9. (a) Fluctuations in the CH Raman signature from PA (gray line) and OH signal from water (black line). (b) Time dependence of the WGM wavelengths observed in the Raman fingerprint over the same time window as part a. (c) Time dependence of the droplet size estimated from the pattern of WGMs shown in part b.

are very different when the inclusion sits toward the droplet edge to in the droplet center, the autocorrelation functions measured can be considered to be consistent with diffusion of the inclusion throughout the droplet volume.

An example of the fluctuations in Raman intensity between 1420 and 1525 s is shown in Figure 9a. It is clear in this time window that the intensities of the CH and OH signatures are inversely correlated. Further, the fluctuations in Raman intensity occur at the same time as fluctuations in the fingerprint of WGM

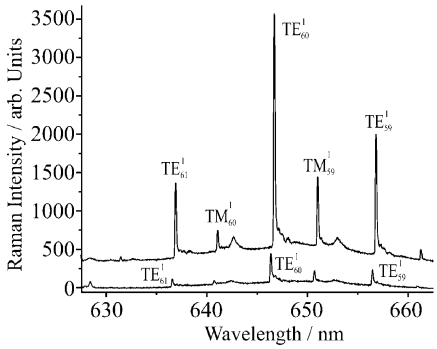

Figure 10. Comparison of the Raman fingerprints at 1450 s when the droplet size is resonant with the incident laser wavelength (top spectrum) and at 1483 s when the droplet size is not resonant. The absolute intensities can be directly compared.

wavelengths, Figure 9b, and hence droplet size, Figure 9c. The droplet size appears to repeatedly rise to an upper limit of 5.01 μm in radius but appears unable to increase above this limit, undergoing periodic excursions to smaller size by ~3 nm. This small size variation is apparent from the similarity of the two spectra recorded at times of 1450 and 1483 s, shown in absolute intensities in Figure 10. Although the size variation is very small, the absolute intensity of the Raman scatter is significantly different. Both the marked enhancement in intensity and the stability of the upper size are a consequence of the droplet size tuning into resonance with a WGM at the laser wavelength.[38,39] At the upper limit of size, enhanced coupling of the illumination wavelength into a WGM leads to enhanced Raman signal from the aqueous phase occupying the WGM volume. The signal from the organic is low, as the inclusion must be absent from the mode volume for the mode quality to be sustained, although a very minor level of stimulated Raman is observed at WGM wavelengths within the CH band. When the droplet size decreases by ~3 nm, the stimulated Raman signal from water diminishes, concurrent with a rise in the spontaneous Raman signature from the PA, giving rise to the inverse correlation in signal magnitude reported in Figure 9 and suggesting that the PA inclusion is repeatedly moving in and out of the trapping beam.

The apparent stability of the upper size reflects the influence of the resonance in determining the vapor pressure of the droplet. Small changes in size as the droplet tunes in and out of resonance with the incident light can lead to significant changes in vapor pressure as the absorption efficiency changes by orders of magnitude, thereby changing the droplet temperature.[39] The droplet size (determining the solute concentration) and temperature act in combination to determine the droplet vapor pressure in order to balance the surrounding partial pressure of water, the RH. Resonant absorption leads to enhancement of temperature and a depression of droplet size, leading to the observation of bistability in droplet size.[40,41] The repeated attempts by the droplet to cross the Mie resonance suggest that the equilibrium droplet size required to match the surrounding environmental conditions tends to have larger size, when governed by the solute concentration and nonresonant heating alone. However, the contribution of resonant heating allows the droplet to attain a steady size, smaller than expected, but with a vapor pressure that balances the surrounding RH through temperature elevation.

The droplet size stability is consistent with previous observations of growing homogeneous water droplets.[39] However, the repeated excursions away from this stable size appear to be consistent with the organic inclusion moving onto the beam axis, leading to the appearance of a spontaneous Raman band. This suggests that movement of the inclusion within the droplet is compromising the level of resonant heating. A possible explanation may be marginal changes in the level of nonresonant heating as the inclusion moves on and off the laser beam axis, leading to small fluctuations in temperature and ensuing small changes in droplet size. The time scale for this size fluctuation is governed by diffusional motion of the inclusion within the droplet and diffusional transport of water in the vapor phase. On the time scale of the fluctuations, the inclusion may be expected to diffuse only 1 μm.

6. Conclusions

We have reported a novel strategy for forming mixed solid−liquid aerosol droplets for studies of the chemical and physical properties of mixed phase systems. Specifically, we have introduced a water-insoluble organic component, palmitic acid, into an aqueous sodium chloride aerosol droplet by first solubilizing the organic in ethanol aerosol and by dosing an optically trapped aqueous aerosol with the volatile organic aerosol. In a second experiment, we have introduced submicrometer polystyrene beads to a host water droplet using a similar method.

The influence of the solid inclusion on both the spontaneous and stimulated Raman signatures of the trapped host droplet has been explored. Further, the impact of the position of the weakly absorbing polystyrene inclusion on the wet droplet size has been observed. When the inclusion resides within the trapping laser beam, the droplet size is observed to decrease markedly, consistent with an increase in nonresonant light absorption by the droplet and an elevation of temperature. The size change is compared with model predictions based on a Beer−Lambert law dependence of absorption and the effective medium approximation.[33]

While polystyrene beads are observed to move throughout the droplet volume, consistent with their dispersibility in aqueous surfactant solution, two distinct classes of microphysical partitioning of PA inclusions within a host aqueous droplet have been observed. The dominant position appears to be for a PA hydrated crystal to adopt a surface configuration; this is consistent with the hydrophobicity of PA and results when the inclusion is observed to form immediately on coalescence. However, the dispersal of PA aggregates within the droplet bulk is also observed, and it is not possible to resolve if these are formed following ethanol evaporation or through direct inclusion by impaction. Inclusion within the bulk could be consistent with the interplay of optical forces exerted on the organic inclusion and the formation of a PA monolayer at the droplet surface reducing the surface tension of the droplet. The motion of the PA inclusion has been investigated by examining the autocorrelation of fluctuations in the Raman intensity, which suggests that the inclusion undertakes motion throughout the whole droplet volume. Finally, the influence of resonant-absorption on the equilibrium size of the host droplet has been observed. Motion of the inclusion into the probe laser volume correlates with fluctuations in size that arise from temporal fluctuations in the level of nonresonant heating.

This paper represents a first demonstration of a strategy for forming mixed solid−liquid phase aerosol droplets in an optical trap. Further, it demonstrates the potential wealth of information that might be obtained from detailed measurements of the fluctuations in droplet composition and size. There remain many further phenomena that can be explored using this approach, including a further investigation of the influence of the inclusion on the equilibrium size on the host droplet and the kinetics of mass transfer at the droplet surface.

Acknowledgment. A.L. and J.P.R. acknowledge Dr. Jariya Buajarern for undertaking preliminary measurements with the polymer beads. A.L. acknowledges studentship support through a Marie Curie Early Stages Training Network. The EPSRC are also acknowledged for financial support for this research and for Advanced Research Fellowship funding for J.P.R. We also acknowledge Mr. R. Dyer of the Kruss Surface Science Center, based at the University of Bristol, for helpful discussions.

References and Notes

(1) O'Dowd, C. D.; Smith, M. H.; Consterdine, I. E.; Lowe, J. A. *Atmos. Environ.* **1997**, *31*, 73.
(2) Fitzgerald, J. W. *Atmos. Environ., Part A* **1991**, *25*, 533.
(3) Randles, C. A.; Russell, L. M.; Ramaswamy, V. *Geophys. Res. Lett.* **2004**, *31*, L16108.
(4) Ellison, G. B.; Tuck, A. F.; Vaida, V. *J. Geophys. Res. [Atmos.]* **1999**, *104*, 11633.
(5) Rudich, Y. *Chem. Rev.* **2003**, *103*, 5097.
(6) Donaldson, D. J.; Vaida, V. *Chem. Rev.* **2006**, *106*, 1445.
(7) Tervahattu, H.; Juhanoja, J.; Kupiainen, K. *J. Geophys. Res. [Atmos.]* **2002**, *107*, 4319.
(8) Garland, R. M.; Wise, M. E.; Beaver, M. R.; DeWitt, H. L.; Aiken, A. C.; Jimenez, J. L.; Tolbert, M. A. *Atmos. Chem. Phys.* **2005**, *5*, 1951.
(9) *Handbook of Chemistry and Physics*; 87th ed.; CRC Press LLC: Boca Raton, FL, 2006−2007.
(10) Bronk, B. V.; Smith, M. J.; Arnold, S. *Opt. Lett.* **1993**, *18*, 93.
(11) Videen, G.; Pellegrino, P.; Ngo, D.; Videen, J. S.; Pinnick, R. G. *Appl. Opt.* **1997**, *36*, 6115.
(12) Krieger, U. K.; Braun, C. *J. Quant. Spectrosc. Radiat. Transfer* **2001**, *70*, 545.
(13) Krieger, U. K.; Corti, T.; Videen, G. *J. Quant. Spectrosc. Radiat. Transfer* **2004**, *89*, 191.
(14) Prabhu, D. R.; Davies, M.; Videen, G. *Opt. Expr.* **2001**, *8*, 308.
(15) Secker, D. R.; Kaye, P. H.; Greenaway, R. S.; Hirst, E.; Bartley, D. L.; Videen, G. *Appl. Opt.* **2000**, *39*, 5023.
(16) Videen, G.; Ngo, D.; Chylek, P.; Pinnick, R. G. *J. Opt. Soc. Am. A:* **1995**, *12*, 922.
(17) Tuckermann, R.; Bauerecker, S.; Cammenga, H. K. *J. Colloid Interface Sci.* **2007**, *310*, 559.
(18) Krieger, U. K.; Zardini, A. A. *Faraday Discuss.* **2008**, *137*, 377.
(19) Mitchem, L.; Reid, J. P. *Chem. Soc. Rev.* **2008**, *37*, 756.
(20) Reid, J. P.; Meresman, H.; Mitchem, L.; Symes, R. *Int. Rev. Phys. Chem.* **2007**, *26*, 139.
(21) Butler, J. R.; Mitchem, L.; Hanford, K. L.; Treuel, L.; Reid, J. P. *Faraday Discuss.* **2008**, *137*, 351.
(22) Reid, J. P.; Mitchem, L. *Annu. Rev. Phys. Chem.* **2006**, *57*, 245.
(23) Buajarern, J.; Mitchem, L.; Reid, J. P. *J. Phys. Chem. A* **2007**, *111*, 9054.
(24) Mitchem, L.; Buajarern, J.; Ward, A. D.; Reid, J. P. *J. Phys. Chem. B* **2006**, *110*, 13700.
(25) Mitchem, L.; Buajarern, J.; Hopkins, R. J.; Ward, A. D.; Gilham, R. J. J.; Johnston, R. L.; Reid, J. P. *J. Phys. Chem. A* **2006**, *110*, 8116.
(26) Wang, X. B.; Shen, Z. X.; Tang, S. H.; Kuok, M. H. *J. Appl. Phys.* **1999**, *85*, 8011.
(27) Mendelsohn, R.; Moore, D. J. *Chem. Phys. Lipids* **1998**, *96*, 141.
(28) De Gelder, J.; De Gussem, K.; Vandenabeele, P.; Moens, L. *J. Raman Spectrosc.* **2007**, *38*, 1133.
(29) Hill, S. C.; Saleheen, H. I.; Fuller, K. A. *J. Opt. Soc. Am. A:* **1995**, *12*, 905.
(30) Teraoka, I.; Arnold, S. *J. Opt. Soc. Am. B:* **2006**, *23*, 1381.
(31) Lin, H. B.; Huston, A. L.; Eversole, J. D.; Campillo, A. J.; Chylek, P. *Opt. Lett.* **1992**, *17*, 970.
(32) Ma, X. Y.; Lu, J. Q.; Brock, R. S.; Jacobs, K. M.; Yang, P.; Hu, X. H. *Physics in Medicine and Biology* **2003**, *48*, 4165.
(33) Knox, K. J.; Reid, J. P. *J. Phys. Chem. A* **2008**, *112*, 10439.
(34) Li, Y.; Pham, J. Q.; Johnston, K. P.; Green, P. F. *Langmuir* **2007**, *23*, 9785.
(35) Tufvesson, F.; Wahlgren, M.; Eliasson, A. C. *Starch-Starke* **2003**, *55*, 138.
(36) Inaba, A. *Bull. Chem. Soc. Jpn.* **1950**, *23*, 146.
(37) Brzozowska, I.; Figaszewski, Z. A. *Colloids Surf., B* **2003**, *30*, 187.
(38) Symes, R.; Sayer, R. M.; Reid, J. P. *Phys. Chem. Chem. Phys.* **2004**, *6*, 474.
(39) Miles, R. E. H.; Reid, J. P.; Guillon, M.; Mitchem, L.; McGloin, D. *Phys. Chem. Chem. Phys.* **2009**, DOI: 10.1039/B904690A.
(40) Arnold, S.; Leung, K. M.; Pluchino, A. *Opt. Lett.* **1986**, *11*, 800.
(41) Arnold, S.; Okeeffe, T. R.; Leung, K. M.; Folan, L. M.; Scalese, T.; Pluchino, A. *Appl. Opt.* **1990**, *29*, 3473.

JP902248P